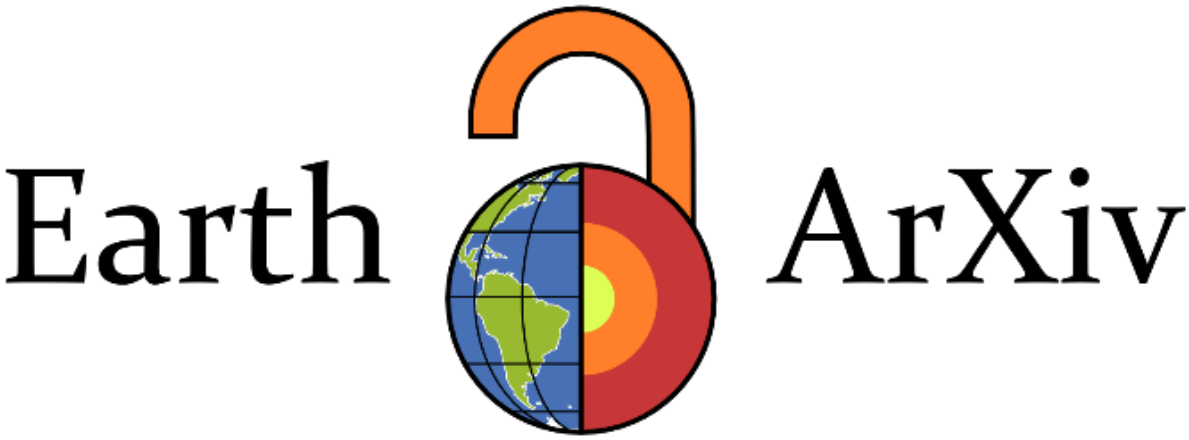

Self Super-Resolution of Time-Separated Multispectral Bands

Ankur Garg, Space Applications Centre **(Corresponding Author),**
Contact : agarg@sac.isro.gov.in
Meenakshi Sarkar, Space Applications Centre
S. Manthira Moorthi, Space Applications Centre
Debajyoti Dhar, Space Applications Centre

Declarations

Conflict of Interest The authors declared that they have no conflict of interest.

Funding N/A

Acknowledgment

The authors thankfully acknowledges the understanding, encouragement and support received from Director, Space Applications Centre, ISRO. The authors would also like to thank other Signal and Image Processing Area (SIPA) members who have given their support from time to time. The continuing support from IRS project Management through IRS Program Director, Cartosat-2S Project Director, Associate Project Director, Payloads, Applications and Ground Segment Committee members is thankfully acknowledged.

Self Super-Resolution of Time-Separated Multispectral Bands

Ankur Garg, Meenakshi Sarkar, S. Manthira Moorthi, Debajyoti Dhar

ARTICLE HISTORY
Compiled November 25, 2024

ABSTRACT
The usual system design compromise in high resolution satellites is to have a higher spatial resolution panchromatic (PAN) channel with 3 or 4 lower spatial resolution multispectral (MX) channels and generate a high spatial & spectral resolution product on ground by making use of the fusion techniques. Since the telescopes of such systems are designed to cater to modulation transfer function (MTF) requirements of higher resolution PAN channel, the MX channels generally have high MTF value at their Nyquist frequency and hence the data is aliased. Also, the general design in such systems is to keep along track separation between MX detectors in the focal plane which results in these channels seeing the same target on ground one after the other with time separation. Due to this design choice, multiple factors such as relative change in satellite attitude, effect occurring by differing look angles and elevation of the terrain, and misalignment occurring due to slight rotation that can occur between detectors placements of these channels. contribute to sub-pixel shifts between MX channels during inorbit imaging. This paper proposes an approach to increase the resolution of MX channels without using any high resolution auxiliary channel, by exploiting high MTF present in the MX channels and misregistration arising due to imaging time separation. A new prior which can be used to adaptively preserve edges and reduce noise simultaneously, a method which increases the robustness in point spread function (PSF) estimation from stellar have also been proposed. Experiments show that the resolution of MX can be improved from 1.6m to 1m without using any PAN band for ISRO's Cartosat-2E i.e. self-superresolution. Our method is generic and can be applied to data from any satellite. The method is especially useful for increasing the resolution of satellites which have only multispectral channels without a higher resolution panchromatic channel.

KEYWORDS
Super Resolution, Cartosat-2E, Point Spread Function, Registration, Fusion, Clustering, ERGAS

1. Introduction

High spatial and spectral resolution remote sensing images are needed to improve the accuracies of cartographic applications. Achieving both high resolution spectral and spatial from the same payload is a design tradeoff. To overcome this issue, a general system design compromise in high resolution satellites is to have a high spatial resolution PAN channel and 3 or 4 low spatial resolution MX channels and generate a high spatial and spectral resolution product using the fusion procedure like that in SPOT-5(1), Pleides(2). Such systems carry same telescope for imaging both PAN and

All authors are with Signal and Image Processing Group, Space Applications Center, Indian Space Research Organisation, Ahmedabad, India-380015, Corresponding email ids : (agarg, pabhishek, meenakshi, smmoorthi, deb)@sac.isro.gov.in

MX channels. Since the telescopes of such systems are designed to cater to modulation transfer function (MTF) requirements of higher resolution PAN, the MX channels generally have high MTF value at their Nyquist frequency and are hence aliased. Also, these systems generally make use of multiple devices to cover the swath requirements. Also, they are usually separated in focal plane in along track direction and hence see same target on ground one after the other with some time lag inorbit. Due to this, sub-pixel shifts between MX channels can occur due to relative change in satellite attitude values, due to effect occurring by differing look angles and elevation of the terrain, and due to misalignment occurring due to slight rotation that can occur between devices of various channels. In the cases where the satellite doesn't contain PAN and MX channels on the same platform, the usual method is to use data from other satellites to generate high resolution MX data using fusion techniques, but geometric differences arising due to misregistration and radiometric deviations due to different radiometry and climatic conditions create problem with such an approach. The advantage of having PAN and MX on the same platform solves the radiometric issues related to differing climatic condition but geometric issues still persists due to imaging time separation and use of multiple devices for each channel to cover full swath.

This paper proposes an approach to increase the resolution of MX channels without using any high resolution auxiliary channel by exploiting high MTF present in the MX channels and misregistration arising between these channels due to imaging time separation. The paper also proposes a new prior which can be used to adaptively preserve edges and reduce noise simultaneously. A method which increases the robustness in point spread function (PSF) estimation from stellar data with respect to previous methods has also been described. The proposed superresolution algorithm uses the available system level knowledge to its fullest by making use of physical geometric model, satellite attitude and PSF estimated from stellar, and is therefore robust enough for operationalization as compared to previous approaches. The MX channels are used to create a psuedo high resolution PAN channel which is then used to fuse with the upsampled low resolution MX images to increase their resolution.

The technique has been used to increase the resolution of Cartosat-2E (C2E) (3) MX images and has been compared to that generated by fusing MX and PAN images. C2E, launched on 23 June 2017 into a 505-kilometre Sun-synchronous orbit is developed by the Indian Space Research Organisation (ISRO). It is designed to collect high-resolution large-scale imagery for use in urban planning, infrastructure development, utilities planning, and traffic management. The satellite is designed to collect high resolution imagery in panchromatic (PAN) channel with ground sampling distance (GSD) of 0.65m and with 1.6m GSD in 4 multispectral (MX) channel with 11 bit data quantization. Four multi-spectral channels are physically separated by 0.00681m in focal plane in along-track direction and with a time delay of 0.0862s between the acquisition of first and last channel. With the integration time of 223 microsecond, shift in first to last channel is around 387 scanlines and they are hence natively unregistered. Full swath of 10km is covered by optical butting(3) 5 devices in each channel. Our algorithm is able to increase the spatial resolution of multispectral data from 1.6m to 1m without using any PAN data.

2. Related Work

Over the last several decades, various super resolution methods have been reported in the literature. The methods can be divided into fourier based (4), non-uniform

interpolation based(5), iterative back projection based(6), projection on convex sets (POCS) based(7), maximum a posteriori (MAP) based(8) and very recently learning based methods(9). Among those MAP based approaches find special place in literature since they allow the image formation formulation to be incorporated along the prior knowledge by making use of regularization. In general, the MAP based methods can be divided into two categories. First category is based on variation in fidelity term. The poisson noise model which is generally followed by images acquired by Charged Coupled Devices (CCD), can be approximated by Gaussian noise model. L2 norm based fidelity model which arise from gaussian noise assumption is the appropriate model to handle this case. Because it penalizes the error in a quadratic manner, their performance is degraded in the presence of outliers such as salt and pepper noise, transmission loss. In case of outliers, L1 norms which comes by white laplacian noise assumption seems to work better as was shown in(10). Also, it is more robust to registration errors. The major disadvantage of L1 norm is that it produces more observation error, is non-differential and can destroy small textures thereby producing overly smooth images leading to loss of information which can be detrimental for remote sensing images. Recently, M-estimators such as Huber functions(11) which can act as both as L1 and L2 norm based on decided threshold have been used to replace fixed norms. The second category of MAP estimate is based on variation in prior. Prior information is added to the cost function to get the desired solution. Regularizers based on L1 based Total Variation (TV)(12) norm, Tikhonov (TV)(13) norm, sparsity based L1 norms including Bilateral TV (BTV)(10) have been proposed. Adaptive version of these norms to reduce noise and at the same time enhance the edge information have been recently proposed such as those based on difference curvature for BTV(14) and TV(15).

Some research endeavors have aimed to train deep learning models using simulated datasets, where Low-Resolution (LR) images are generated using a predefined degradation model (16). However, the effectiveness of these models may decline considerably if the real low-resolution input deviates from the simulated degradation model. Other approaches incorporate real HR images obtained from different satellites to directly guide the Super-Resolution (SR) process of a coarse resolution satellite like Sentinel-2 [(17), (19), (18)]. Nevertheless, acquiring HR ground truth images can be financially demanding. Furthermore, the utilization of HR images from diverse satellites introduces challenges, including spectral response variations, differences in acquisition viewpoint and time. These complexities complicate the dataset creation process and have a detrimental impact on overall performance. Also they suffer from "hallucination" effect where the model may generate information which may not be present in the real world. Certain methodologies, such as the one outlined in (20), employ self-supervision for model training but exhibit a pronounced reliance on the specific hardware imaging acquisition strategies. As an illustration, the utilization of overlapping regions is restricted to early products within the Sentinel-2 processing pipeline, specifically in the level-1B (L1B) products. These early products introduce a notable interband parallax, a consequence of the hardware design of detectors aimed at enhancing the resolution of Sentinel-2 images.

In operational satellite data processing, super resolution has been used in SPOT-5 HRG(21) to increase the spatial resolution from 5 meters(m) to 3m. Skybox(22) also uses algorithm to generate high resolution channel from video acquisitions. Both the satellites acquire images from lower earth orbit. These super-resolution algorithm works on the assumption that the low-resolution images are single channel and come from same radiometry.

The approach described in the paper exploits high MTF present in the MX-channels and misregistration arising between channels due to imaging separation. The technique uses robust system level models by incorporating the point spread function (PSF) derived using stellar observations and geometric model refined with image matching to determine shifts at sub-pixel level between channels and the observation model with takes into account the differing radiometry of the channels similar to (23). The paper proposes a new prior which can be used to adaptively preserves edges and reduces noises at the same time and creates a psuedo high resolution PAN channel. Finally this PAN channel is used to fuse the upsampled with the low resolution MX images to increase their resolution using smoothing-filter-based intensity modulation (SFIM)(24).

3. Proposed Model

Our observation model for deriving low resolution MX channels from high resolution PAN channel is similar to that defined in (23) for hyperpsectral images and is given by Equation 1

$$Y_k = S_k D M_k B_k X + N_k \tag{1}$$

where subscript k denote the k^{th} MX channel, the matrix Y_k is the low resolution MX channel of size $N \times M$, X is the high resolution PAN channel of size $sN \times sM$ where s is the scaling factor, B_k is the high resolution point spread function i.e. the blur which high resolution image undergoes before sampling to produce the corresponding channel, M_k is the motion matrix containg misregistration information between different channels, D is the decimation matrix and S_k is the spectral coefficient matrix which maps the high resolution pseudo PAN channel to low resolution MX channels of specific radiometry and N_k is the noise matrix corresponding to low resolution MX channel. Given n such low resolution MX channels of differing radiometry, the high resolution PAN channel X can be derived by minimizing Equation 2

$$argmin \sum_{k=1}^{n} ||Y_k - S_k D M_k B_k X||_p^p + \phi(X) \tag{2}$$

where the first part of the equation is the likelihood term with norm p and $\phi(X)$ is the prior probability of the desired solution in the MAP framework. $p = 2$ corresponds to Gaussian noise model assumption, $p = 1$ corresponds to laplacian noise model assumption and $p < 1$ correspond to hyper Laplacian ones. As discussed in the last section, the prior model $\phi(X)$ can take the form of $L2$ norm, $L1$ norm, BTV norm or Lp norm where $p < 1$ (**?**) for enhancing sparsity. Having defined the generic observation model, following subsection discusses how values for each of the above terms are being derived.

3.1. *High Resolution PSF (B_k):*

The MTF degradation in satellite images occur due to the diffraction limit of the telescope, optical distortions, the detector footprint blur and the smear effect occuring due to relative motion between satellite and object being imaged. The PSF for each

MX channel is different beacuse the optical blur is different for each. To get the high resolution blur function for each channel, stellar images have been acquired by steering the satellite to point to stars thanks to the agility of C2E platform. Multiple such stellar images have been interlaced to a common high resolution grid of sampling S by first choosing a star as a reference, then deriving subpixel shifts between the reference star and other stars by performing normalized cross correlation (NCC), then applying quadratic fit on the correlation surface and registering all stars to this reference. All the stars are interpolated to high resolution grid by interpolating them by sinc interpolter to cause minimum degradation in terms of MTF, and merged by averaging their response. Finally the derived response is centered after finding its centroid and translating by the derived subpixel shift. We find that this approach of first registering the stars to a common star, interpolating, merging them and then centering the final merged result by computing its centroid is far robust to noise as compared to the approach discussed in (25), where first the centroid of all the stars are derived, each one is centered , finally interpolated and merged simply because NCC is more robust to noise as compared to centroid computaion and performing centroiding at the merged response level increases its robustness as the noise decreases due to averaging the response of all the stars. To verify the efficacy and compare the two methods, simulations were carried out with 18 stars by introducing various subpixel shifts in Gaussian shape PSF under various noise conditions. Figure 1 shows the result for one such case, where Method-1 refers to the method we discuss here and Method-2 to that defined in (25). It can be clearly seen that Method-1 is able to derive the sub-pixel shift better as compared to Method-2 and the derived shifts are more closer to the reference. Table 2 shows the mean absolute error (MAE) in the derived shifts under various noise conditions. It can be clearly seen that Method-1 performs better than Method-2 in all the cases and works even under extreme noise conditions whereas Method-2 gives large errors in estimating the subpixel shifts, which finally leads to error in the generated point spread function.

Table 1. Comparison of Methods

Noise (σ)	**Method-1 MAE (pix)**	**Method-2 MAE (pix)**
0.02	0.228	0.546
0.01	0.035	0.419
No Noise	0.037	0.403

3.2. *Motion Matrix (M_k):*

Sub-pixel shifts between the imaging channels is of prime importance for any super resolution algorithm to work. The sub-pixel shifts can be computed using solely image processing techniques like that proposed in optical flow(26). These approaches are fully image based and don't required knowledge of the actual sensing geometry of the image but they can fail in the presence of severe clouds and water, are very sensitive to outliers and can cause local distortions in the derived motion surface. To account for the same, a hybrid image processing and geometric model based approach is used where the relative attitude profiles between channels in roll, pitch, yaw are modelled in terms of in terms of biases and the linear rate. In satellite data processing, physical geometric model aims at computing the ground location of every pixel at a given time based on telemetry data i.e. orbital ephemeris (state vector and velocity), attitude data (orientation in the form of roll, pitch and yaw angles), imaging time stamps, calibrated

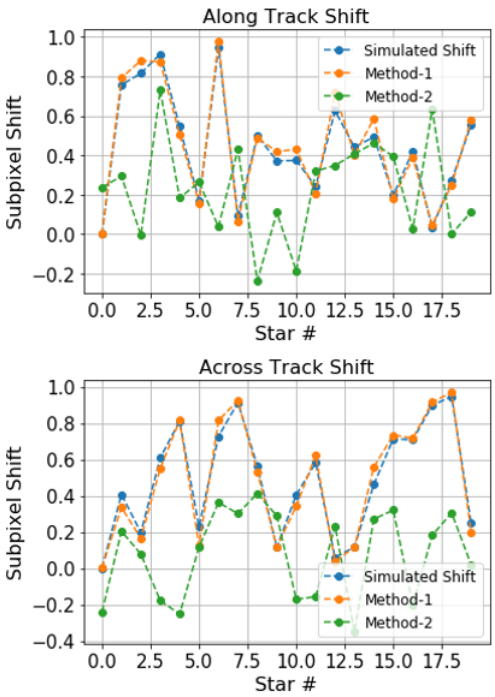

Figure 1. Comparison between Stellar Estimation Methods

instrument parameters and elevation of the terrain derived from digital elevation model (DEM). This model is called "image to ground model". Given the ground location on the ground, it also helps to compute the scan and pixel position which sees that ground position, this is "image to ground model". In this approach, first the source channel is divided in predefined number of square non-overlapping blocks. Each square block is then searched, in the reference channel at the same location assuming a certain search space and desired subpixel shift is derived by quadratic fit on the correlation surface generated by normalized cross correlation. After performing this process for each block, the outliers are rejected by Random Sample Consensus (RANSAC) (27) by fitting affine model in the generated match points. Using the derived correspondences, the roll, pitch, yaw orientations are refined with space resection process (28). Finally the motion matrix between channels is computed for each scan and pixel in the image by calling "image to ground model" of source channel to generate latitude/longitude information and then using those latitude/longitude information to find which reference channel scan and pixel will see that ground point using "ground to image model". The process is repeated to derive scan and pixel error grids for each channel with respect to red channel, which is taken here as a reference. Figure 2 shows the scan and pixel error grids for three channels with respect to red channel derived using the same approach. These derived errors are interlaced in processing and help in generating the required phase shift needed for super resolved image creation.

3.3. *Spectral Coefficient Matrix (S_k):*

The spectral coefficient for a certain channel is computed by registering all other channel with respect to this channel and then calculating coefficients as defined in (23), which is given in Equation3.

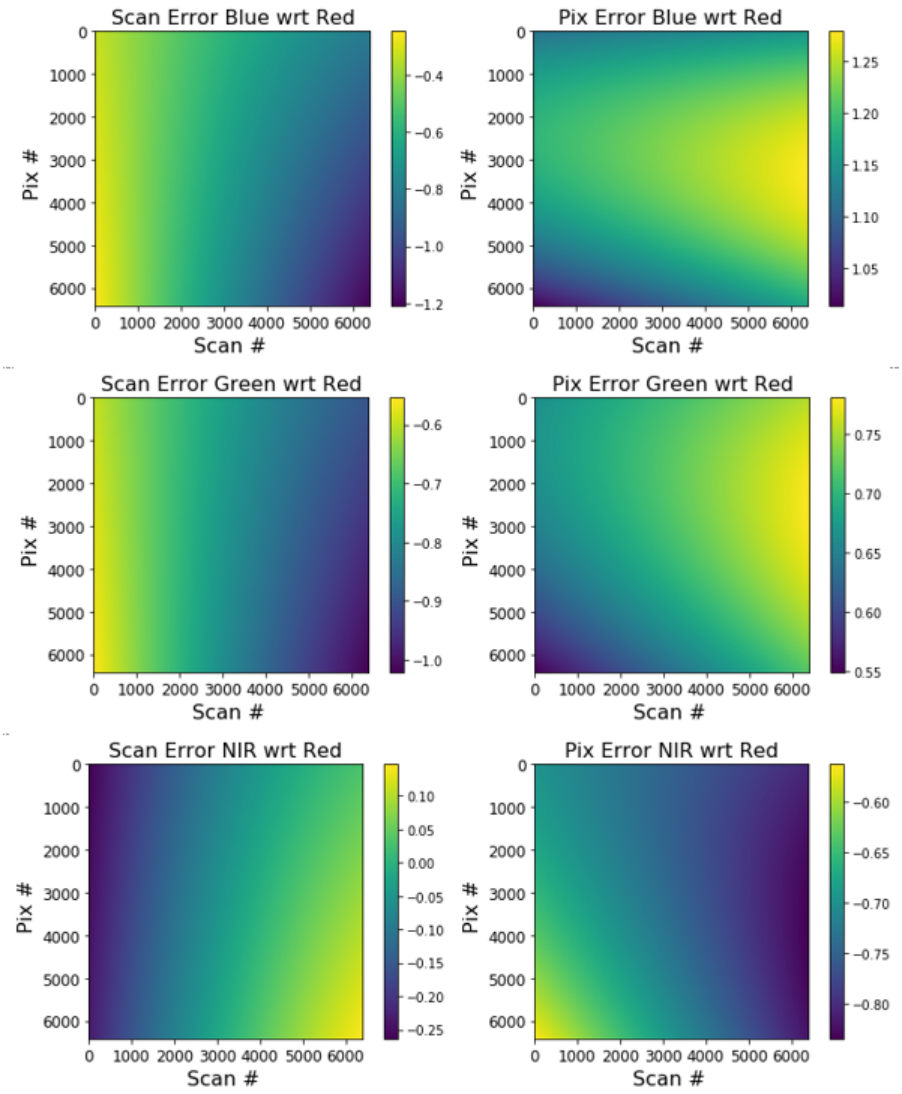

Figure 2. Scan and Pix Errors

$$S_k(i) = I_k(i)/(I_k(i) + \sum_{j \neq k, j=1}^{n} I_j^{'}(i)) \tag{3}$$

where $I_k(i)$ is the channel for which the spectral coefficient is being estimated, and $I_j^{'}(i)$ are other channels which have been registered to this channel. The spectral coefficients are computed after converting the original digital number(DN) obtained from instrument to radiance value as not doing so and using DN value will result in artifacts in the final image since the DN is property of the instrument and is not a physical quantity.

3.4. *Prior Model ($\phi(X)$):*

We use BTV operator as the prior model as it preserves edges in our algorithm and also has fewer smoothing effects. The BTV operator is given by Equation 4

$$BTV(X) = \sum_{l=-P}^{P} \sum_{m=0,l+m>0}^{P} \alpha^{|m|+|l|} ||X - S_h^l S_v^m X|| \tag{4}$$

where S_h^l and S_v^m are a translated form of X by l and m pixels in the horizontal and vertical directions respectively. Weight factor α provides spatially decaying effect to regularization. To better preserve edges and textures which are very critical for remote sensing images, we propose to use adaptive weighted BTV prior based on Rmap as given by Equation 5. Rmap was first proposed in (29) to preserve edges and remove smooth regions for kernel estimation. A large value of r indicates that edge with large magnitude exists and small value means that it is relatively smooth region. Figure 3 shows Rmap for one such image patch. The histograms for original image and Rmap after scaling to 0-1 has also been shown. Rmap shows value close to 1 when sharp transitions in the form of edges are present and value close to 0 in the presence of smooth regions. This prior has been used for edge-preserving filter in (30) but this is the first time that this prior has been deployed in the context of super resolution.

$$w(i) = \exp(-||r(i)||^{0.8}) \tag{5}$$

where $r(i)$ is the Rmap value for the corresponding pixel.

$$r(i) = \frac{||\sum_j \nabla I(i)||_2^2}{\sum_j ||\nabla I(i)||_2^2 + 0.5} \tag{6}$$

where j is a loop which runs in the neighbour of pixel i.

3.5. *Likelihood Term :*

Because we use robust system level model to estimate registration error and correct for any salt and pepper noise or transmission loss before super resolution, we don't make use of L1 norm but rather use L2 norm as the likelihood term as it is optimal and preserves the textures better. Experiments show that L2 norm performs better than L1 with respect to the sharpness as shown in next section.
Equation 7 describes the complete minimization function for the whole framework for super resolving multispectral images.

$$\begin{aligned} \hat{X} = argmin \sum_{k=1}^{n} ||Y_k - S_k D M_k B_k X||_2^2 + \\ \lambda w \sum_{l=-P}^{P} \sum_{m=0,l+m>0}^{P} \alpha^{|m|+|l|} ||X - S_h^l S_v^m X|| \end{aligned} \tag{7}$$

where λ is the parameter to control the strength of regularization parameter as compared to likelihood term.

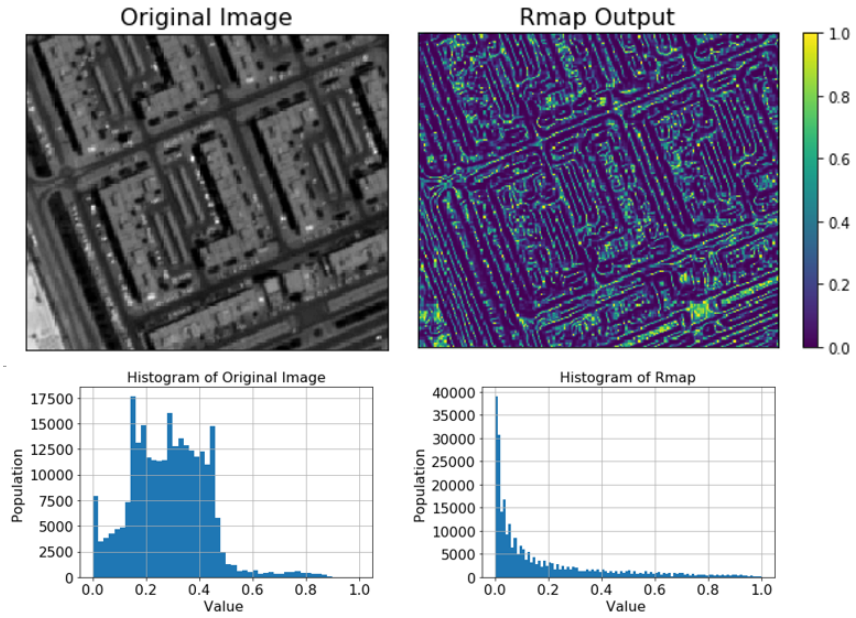

Figure 3. Adaptive Prior Model Based on Rmap

The above equation is solved using iterative steepest gradient algorithm. Differentiating the above equation with respect to X and putting the derivative to 0 gives the following iterative solution.

$$\hat{X_{n+1}} = \hat{X} - \beta\Big\{ \sum_{k=1}^{n} M_k^T B_k^T D_k^T S_k^T (Y_k - S_k D M_k B_k X) + \lambda w \\ \sum_{l=-P}^{P} \sum_{m=0,l+m>0}^{P} \alpha^{|m|+|l|} (I - S_h^{-l} S_v^{-m}) sign(\hat{X} - S_h^l S_v^m \hat{X}) \Big\} \tag{8}$$

where β is the learning rate which is changed adaptively for faster convergence by following scheme. If the cost of the current iteration is lesser than previous iteration, the learning rate is increased by 5%, if more than the last iteration, the learning rate is decreased by 5% and if it is within 1% with respect to previous one for 3 iterations, then the convergence is reached, loop is broken and the solution is returned. The generated high resolution PAN channel is fused with lower resolution channels using smoothing-filter-based intensity modulation(SFIM) fusion technique to generate high resolution MX channels.

4. Experiments and Results

The algorithm has been implemented in Nvidia Tesla K40 GPU card in CUDA and each iteration takes ∼3seconds for doubling the resolution of 4 MX channels each having ∼36 million pixels. In all experiments, the learning rate β has been set as 0.8, the regularization parameter λ has been set to 0.015, gradient weight α term for BTV has been set to 0.2 and (l, m) to (4,4), with maximum number of iterations being 30. These parameters have been determined by experimentation, but are found to perform

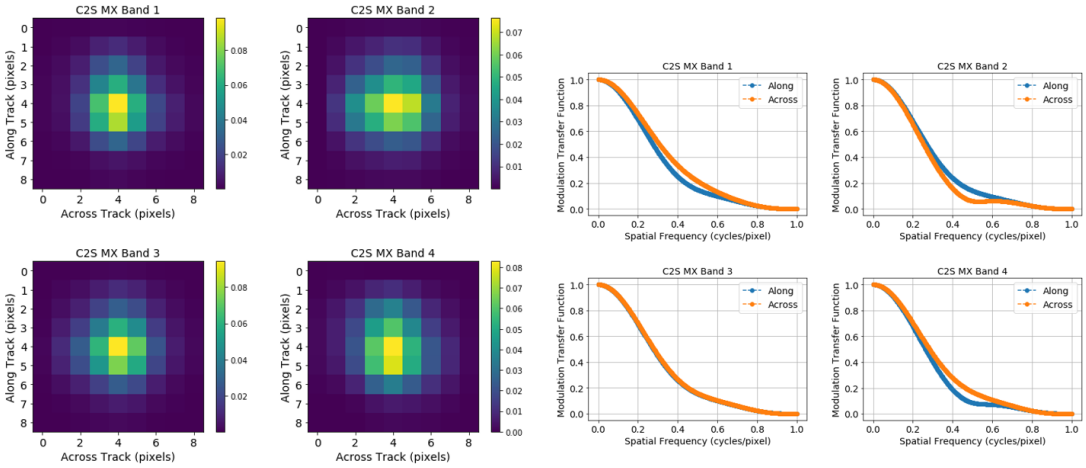

Figure 4. Derived Point Spread Functions and Modulation Transfer Function

optimally for all cases.

Modulation Transfer Function and sub-pixel shifts are the two governing factors for the final spatially resolved image or the so called limit of superresolution. Figure 4 shows the point spread functions and modulation transfer functions derived from Cartosat-2E stellar data using the algorithm described in the previous section.

The MTFs for different bands show that it has value of 15-18% at Nyquist frequency. It is also clear from the MTF that telescope doesn't have the capability to cater to double the nyquist frequency. Hence the spatial resolution cannot be doubled because the telescope is not catching enough spatial frequencies. MTF values goes to zero at around 0.75 cycles/pixel (i.e. 1m) for almost every channel, and hence that is the limit of super resolution for this case. We thus generate super resolved image at 1m spatial resolution and compare the performance with fused image generated at 1m with PAN and MX images.

The performance of the super-resolution approach in presence of proposed prior has been compared to the prominent ones by taking L1 or L2 norm as likelihood term and TV, THV, BTV and our ABTV as prior model. Figure 5 shows the visual results of the experiment for three different patches cropped from the processed image. It can be clearly seen that L1+TV, L1+BTV produce very blurry results while L1+THV produces sharper but noisier results. The super resolution performance increase with L2 norm as likelihood term. L2+TV produces sharper images but noisier image, L2+THV produces artifacts in the form of ringing in the processed image. The best result among the non-adaptive methods is produced by L2+BTV which is able to produce relatively sharper, less noisier and images with less artifacts as shown in second last column, but it still is sub-optimal as it leads to loss of small features as can be seen from the second row parking lot image in the figure. Our proposed method L2+ABTV produces the best visual image as it preserves small textures and also decreases noise in the produced output as is evident from the last column of the figure. The demarcations between cars in the first patch, the parking lot lines in the second patch, and the road markings are visually better in the last column. For performing statistical comparison between these methods and to show how the proposed algorithm can aid in further data and machine analysis, we cluster the image into 3 classes with Kmeans and the results are shown in Figure 6 for the parking lot image. As is evident from the figure, L2+ABTV shown in the last column is able to show parking demarcations better with

less noise in the final classified image.

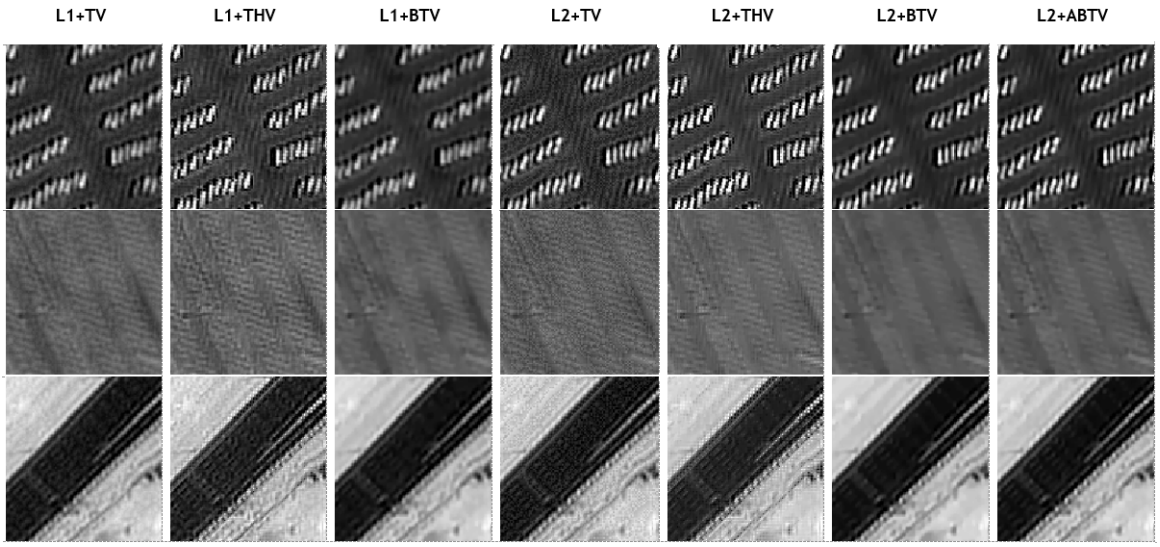

Figure 5. Comparison between Super-Resolution Methods

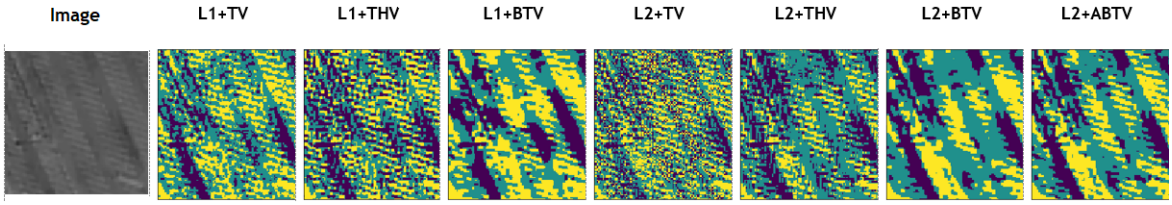

Figure 6. Clustering with 3 classes

To evaluate whether the super resolved image is actually a 1m spatial resolution, a comparison between MX image upsampled with cubic convolution(CC), the generated super-resolved image and PAN image at 1m sampling image is shown in Figure 7. Visually seeing, the cars shown in the first rows are better seen in super-resolved image and is similar in resolvability to panchromatic image. Second row shows that the parking lot is better visible in super resolved image as compared to upsampled MX image. The third row shows the image from farms. The demarcation between fields which are not seen in upsampled MX are clearly visible in super resolved image and are similar to panchromatic image.

To compare the super resolved image statistically, a comparison between super resolved MX image and the fused image generated with 1m PAN image and MX images has been made based on following parameters:

- The **difference in variance (DIV)** measures the quality of derived image by calculating the mean difference in variances between the superresolved/pansharpened image and the original multispectral image.
- **Spectral Angle Mapper (SAM)** measures the cosine of the angle between multispectral and pansharpened/superresolved image to find the similarity.
- The **relative average spectral error index (RASE)** characterizes the aver-

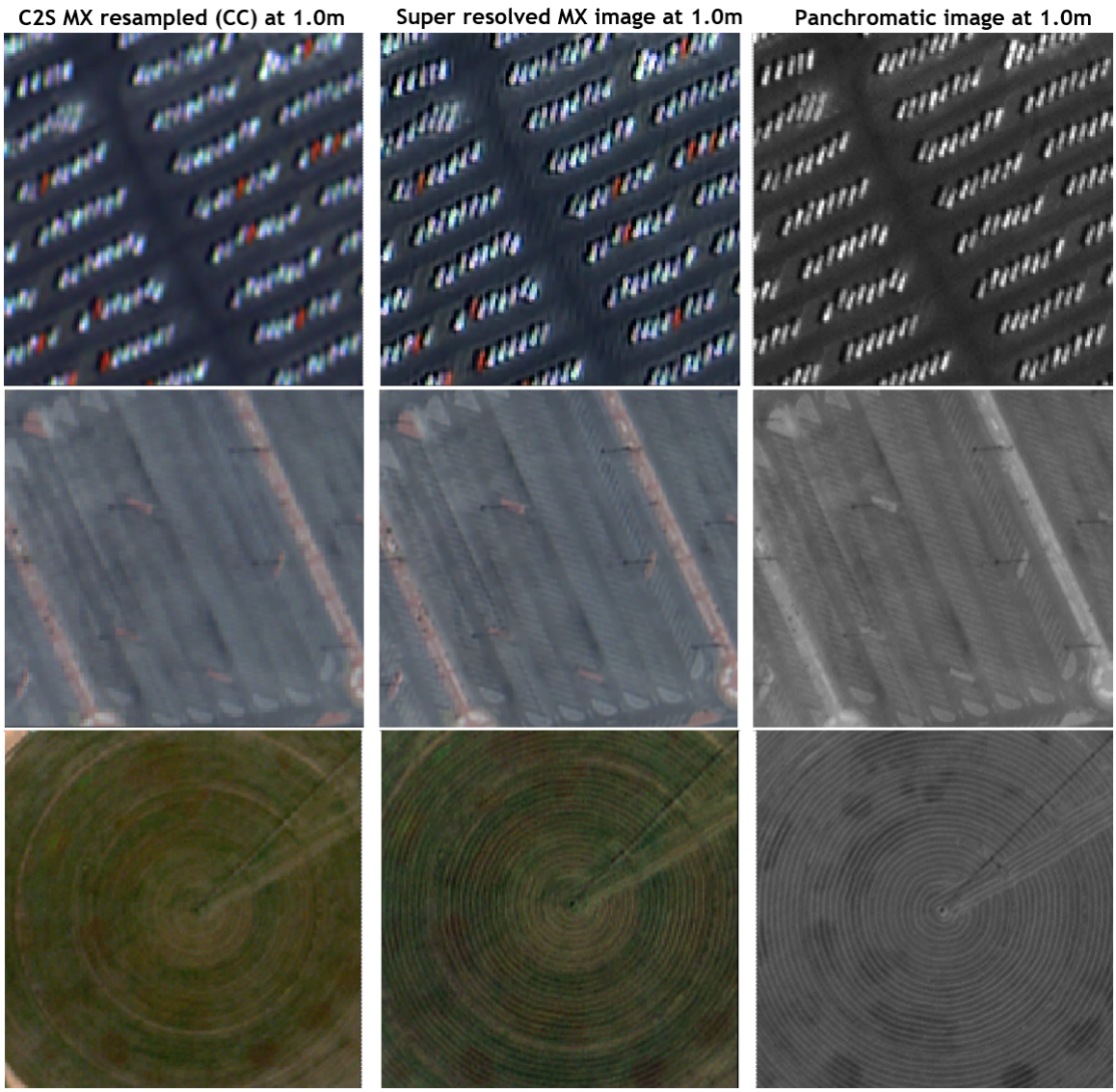

Figure 7. Comparison between Super-Resolution Image and PAN Image at 1m sampling

age performance of the method for all bands:

$$RASE = \frac{1}{\mu}\sqrt{\frac{1}{N}\sum_{i=1}^{N}(DM(R_i)^2 + SSD(R_i)^2)} \tag{9}$$

where μ is the mean of the reference image, R_i is the index of the reference image, SSD is the Standard deviation of the difference image (SSD) relative to the mean of the reference image, and DM is the Difference between the means of the upsampled multispectral images and the merged images.

- **Relative global dimensional synthesis error (ERGAS)**: ERGAS (31) is one of the most popularly used method for image fusion quality estimation.

Equation10 is the formula for computing ERGAS

$$ERGAS = 100 * \frac{h}{l} \sqrt{\frac{1}{N} \sum_{i=1}^{N} \frac{DM(R_i)^2 + SSD(R_i)^2}{\mu_i^2}} \tag{10}$$

where h and l are the resolution of the high and low spatial resolution images, respectively, and μ_i is the mean radiance of each spectral band involved in the fusion process. DM and SSD are defined above in the text. The lower the values of RASE and ERGAS indexes, the higher the spectral quality of the merged images.

- **Gradient Index**: Average gradient index (AG)(32) for spatial quality evaluation. AG describes the changing feature of image texture and the detailed information. Larger values of the AG index correspond to higher spatial resolution.

Table 2. Comparison of Methods

Index	Ideal Value	Fused Image at 1m	SR Image at 1m
DIV (Bandwise)	0.0	0.10, 0.08, 0.06, 0.1	0.00, 0.02, 0.02, -0.02
SAM (Bandwise)	0.0	2.05, 1.64, 1.43, 1.59	0.98, 1.06, 1.05, 0.65
RASE (Bandwise)	0.0	3.66, 2.92, 2.54, 2.82	1.73, 1.87, 1.84, 1.15
ERGAS	0.0	2.26	1.25
Gradient Index	Higher	14.07	13.84

DIV, SAM, RASE and ERGAS are used to compare the spectral performance of the high resolution image and AG is used to compare the spatial performance. Table 2 shows the ideal values for each of the parameters, the value derived for four MX bands for fused and super resolved image. Superresolved is better than the fused image in terms of the spectral indices and comes very close for spatial index. This shows that superresolved image is better or comparable to the fused image at 1m.

5. Conclusion

This paper proposes an approach to increase the resolution of MX channels without using any high resolution auxiliary channel, by exploiting high MTF present in the MX channels and misregistration arising due to imaging time separation. A new prior which can be used to adaptively preserve edges and reduce noise simultaneously, and a method which increases the robustness in point spread function (PSF) estimation from stellar have also been proposed. The super resolved image performance has been compared with respect to fused image generated at 1m in visual sense and also in terms of various spectral & spatial indices and the super resolved is found to be better in spectral and comparable in terms of spatial index. Experiments show that the resolution can be improved from 1.6m to 1m without using any PAN band for Cartosat-2E. The method is generic and can be applied to data from any satellite. The method is especially useful for increasing the resolution of satellites which have only multispectral channels without a higher resolution panchromatic channel.

References

[1] C. Latry, H. Vadon, M. J. Lefevre and H. De Boissezon, "SPOT5 THX: a 2.5m fused product," 2003 2nd GRSS/ISPRS Joint Workshop on Remote Sensing and Data Fusion over Urban Areas, Berlin, Germany, 2003, pp. 87-89, doi: 10.1109/DFUA.2003.1219963.

[2] Laporterie, Florence & Latry, Christophe & Boissezon, Hélène & Lefèvre-Fonollosa, Marie. (2003). Evaluation of the quality of panchromatic / multispectral fusion algorithms performed on images simulating the future Pleiades satellites.

[3] Arti Sarkar, B. Narasiha Sharma, Manish Saxena, Nitesh Thapa, Anand Kumar, Himanshu K. Dave, Somya S. Sarkar, "Development of method for active alignment of multiple time delay and integration detectors in the optically butted focal plane assembly of high-resolution spaceborne imaging systems," J. Appl. Remote Sens. 12(3), 034003 (2018), doi: 10.1117/1.JRS.12.034003.

[4] Huang T.S., Tsan R.Y. Multiple frame image restoration and registration Advances in Computer Vision and Image Process, JAI Press, Inc., Greenwich, CT (1984), pp. 317-339

[5] Komatsu T., Aizawa K., Igarashi T., Saito T. Signal-processing based method for acquiring very high resolution image with multiple cameras and its theoretical analysis Proc. Inst. Electr. Eng., 140 (1) (1993), pp. 19-25

[6] Irani, Michal, and Shmuel Peleg. "Improving resolution by image registration." CVGIP: Graphical models and image processing 53.3 (1991): 231-239.

[7] Stark H., Oskoui P. High resolution image recovery from image-plane arrays, using convex projections J. Opt. Soc. Am. A, 6 (1989), pp. 1715-1726

[8] Lee E., Kang M. Regularized adaptive high-resolution image reconstruction considering inaccurate subpixel registration IEEE Trans. Image Process., 12 (2003), pp. 806-813

[9] Lediga C., Theis L., Huszár F., Caballero J., Cunningham A., Acosta A., Aitken A., Tejani A., Totz J., Wang Z., Shi W.Photo-realistic single image super-resolution using a generative adversarial network CVPR (2017), 10.1109/CVPR.2017.19

[10] Farsiu S., Robinson M.D., Elad M., Milanfar P. Fast and robust multiframe super-resolution IEEE Trans. Image Process., 13 (10) (2004), pp. 1327-1344

[11] Schultz R., Stevenson R. Extraction of high-resolution frames from video sequences IEEE Trans. Image Process., 5 (6) (1996), pp. 996-1011

[12] Ng M., Shen H., Lam E., Zhang L .A total variation regularization based super-resolution reconstruction algorithm for digital video J. Adv. Signal Process. (2007), pp. 1-16

[13] Zhang, Xin, et al. "Application of Tikhonov regularization to super-resolution reconstruction of brain MRI images." International Conference on Medical Imaging and Informatics. Springer, Berlin, Heidelberg, 2007.

[14] Yuan, Qiangqiang, Liangpei Zhang, and Huanfeng Shen. "Multiframe super-resolution employing a spatially weighted total variation model." IEEE Transactions on circuits and systems for video technology 22.3 (2011): 379-392.

[15] Liu, Xiaohong, and Jiying Zhao. "Robust multi-frame super-resolution with adaptive norm choice and difference curvature based btv regularization." 2017 IEEE Global Conference on Signal and Information Processing (GlobalSIP). IEEE, 2017.

[16] Pineda, F., V. Ayma, and C. Beltran. "A generative adversarial network approach for super-resolution of sentinel-2 satellite images." The International Archives of the Photogrammetry, Remote Sensing and Spatial Information Sciences 43 (2020): 9-14.

[17] Liebel, Lukas, and Marco Körner. "Single-image super resolution for multispectral remote sensing data using convolutional neural networks." The International Archives of the Photogrammetry, Remote Sensing and Spatial Information Sciences 41 (2016): 883-890.

[18] Nguyen, Ngoc Long, et al. "On the role of alias and band-shift for sentinel-2 super-resolution." arXiv preprint arXiv:2302.11494 (2023).

[19] Galar, Mikel, et al. "Super-resolution of sentinel-2 images using convolutional neural networks and real ground truth data." Remote Sensing 12.18 (2020): 2941.

[20] Nguyen, Ngoc Long, et al. "L1BSR: Exploiting Detector Overlap for Self-Supervised Single-Image Super-Resolution of Sentinel-2 L1B Imagery." Proceedings of the IEEE/CVF

Conference on Computer Vision and Pattern Recognition. 2023.
[21] Latry, Christophe, and Bernard Rouge. "Spot5 thr mode." Earth observing systems III. Vol. 3439. International Society for Optics and Photonics, 1998.
[22] Kiran Murthy, Michael Shearn, Byron D. Smiley, Alexandra H. Chau, Josh Levine, M. Dirk Robinson, "SkySat-1: very high-resolution imagery from a small satellite," Proc. SPIE 9241, Sensors, Systems, and Next-Generation Satellites XVIII, 92411E (7 October 2014);
[23] Su, Lijuan, Shubo Zhou, and Yan Yuan. "High spatial resolution image restoration from subpixel-shifted hyperspectral images." Journal of Applied Remote Sensing 9.1 (2015): 095093.
[24] Liu, J. G. "Smoothing filter-based intensity modulation: A spectral preserve image fusion technique for improving spatial details." International Journal of Remote Sensing 21.18 (2000): 3461-3472.
[25] Faran, Sagi, et al. "Estimation of the MTF of a satellite imaging-system from celestial scenes." 2009 IEEE International Geoscience and Remote Sensing Symposium. Vol. 2. IEEE, 2009.
[26] XIONG, Jing-Yi, L. U. O. Yu-Pin, and T. A. N. G. Guang-Rong. "An improved optical flow method for image registration with large-scale movements." Acta Automatica Sinica 34.7 (2008): 760-764.
[27] Derpanis, Konstantinos G. "Overview of the RANSAC Algorithm." Image Rochester NY 4.1 (2010): 2-3.
[28] Zeng, Zhuoqiao, and Xibo Wang. "A general solution of a closed-form space resection." Photogrammetric Engineering and Remote Sensing 58 (1992): 327-327.
[29] Xu, Li, and Jiaya Jia. "Two-phase kernel estimation for robust motion deblurring." European conference on computer vision. Springer, Berlin, Heidelberg, 2010.
[30] Fan, Wanshu, et al. "Edge-preserving filter with adaptive L 0 gradient optimization." International Journal of Distributed Sensor Networks 15.2 (2019): 1550147719826946.
[31] Wald, Lucien. "Quality of high resolution synthesised images: Is there a simple criterion?." Third conference" Fusion of Earth data: merging point measurements, raster maps and remotely sensed images". SEE/URISCA, 2000.
[32] Guo, Qing, et al. "Covariance intersection based image fusion technique with application to pansharpening in remote sensing." Information Sciences 180.18 (2010): 3434-3443.